Nanoscale

PAPER

View Article Online
View Journal | View Issue

Cite this: *Nanoscale*, 2018, **10**, 4237

Complete amplitude and phase control of light using broadband holographic metasurfaces†

Gun-Yeal Lee,[a] Gwanho Yoon,[b] Seung-Yeol Lee,[c] Hansik Yun,[a] Jaebum Cho,[a] Kyookeun Lee,[a] Hwi Kim,[d] Junsuk Rho[b,e] and Byoungho Lee *[a]

Received 25th September 2017,
Accepted 28th December 2017

DOI: 10.1039/c7nr07154j

rsc.li/nanoscale

Reconstruction of light profiles with amplitude and phase information, called holography, is an attractive optical technology with various significant applications such as three-dimensional imaging and optical data storage. Subwavelength spatial control of both amplitude and phase of light is an essential requirement for an ideal hologram. However, traditional holographic devices suffer from their restricted capabilities of incomplete modulation in both amplitude and phase of visible light; this results in sacrifice of optical information and undesirable occurrences of critical noises in holographic images. Herein, we have proposed a novel metasurface that is capable of completely controlling both the amplitude and phase profiles of visible light independently with subwavelength spatial resolution. The full, continuous, and broadband control of both amplitude and phase was achieved using X-shaped meta-atoms based on the expanded concept of the Pancharatnam-Berry phase. The first experimental demonstrations of the complete complex-amplitude holograms with subwavelength definition at visible wavelengths were achieved, and excellent performances with a remarkable signal-to-noise ratio as compared to those of traditional phase-only holograms were obtained. Extraordinary control capability with versatile advantages of our metasurface paves a way to an ideal holography, which is expected to be a significant advancement in the field of optical holography and metasurfaces.

Introduction

Holography is an optical technique that reconstructs the wave front of electromagnetic waves with both amplitude and phase information to display three-dimensional (3D) images.[1] Holography has been an attractive topic ever since it has been used to realize ultimate 3D displays and optical data storage.[2–4] However, conventional digital holography techniques, which are based on typical optoelectronic devices such as spatial light modulators and digital micro-mirror devices, have been suffering from several issues, such as low resolution, narrow viewing angle, and severe noises generated from undesirable diffraction orders and twin images, due to their large pixel size as compared to the operating wavelengths. More importantly, conventional holography techniques are usually based on the amplitude- or phase-only modulation scheme with incomplete approximations of object images. In principle, a complex-amplitude modulation, which means independent modulation of both amplitude and phase of light, is required to perfectly reconstruct the profile of light. However, for conventional devices, operating mechanisms of both amplitude- and phase-modulation fundamentally interfere with each other; this causes challenges for independent and full control of them. Although there are a few reports on complex-amplitude modulation schemes applied to the conventional optoelectronic devices, they still suffer from issues including twin image generation, huge optical system size, and limited modulation ranges.[5–9] Hence, despite its significance, implementation of high quality complex-amplitude modulation scheme has not been demonstrated to date.

Metasurfaces, which are planar optical elements with the composition of artificially fabricated photonic atoms, have attracted extensive interest owing to their numerous function-

[a]*School of Electrical and Computer Engineering and Inter-University Semiconductor Research Center, Seoul National University, Gwanak-gu Gwanak-ro 1, Seoul 08826, Republic of Korea. E-mail: byoungho@snu.ac.kr*
[b]*Department of Mechanical Engineering, Pohang University of Science and Technology (POSTECH), Nam-gu Cheongam-ro 77, Pohang 37673, Republic of Korea*
[c]*School of Electronics Engineering, College of IT Engineering, Kyungpook National University, buk-gu daehakro 80, Daegu 702-701, Republic of Korea*
[d]*Department of Electronics and Information Engineering, Korea University, Sejong-ro 2511, Sejong 339-700, Republic of Korea*
[e]*Department of Chemical Engineering, Pohang University of Science and Technology (POSTECH), Nam-gu Cheongam-ro 77, Pohang 37673, Republic of Korea*

†Electronic supplementary information (ESI) available: Supplementary texts with details of numerical simulations, device fabrication, optical measurement, and hologram design. Supplementary Movies S1–S3. See DOI: 10.1039/c7nr07154j

alities and potentials to modify electromagnetic characteristics.[10–14] The applied areas of metasurfaces have been rapidly expanding with noticeable examples including negative index materials and unusual nonlinear optical materials.[15–19] Recently, metasurfaces are expected to pave the path for high quality spatial light modulators that can overcome the limitations of conventional optical components. A number of metasurfaces have been investigated as holographic devices with control of phase,[20–30] polarization,[31] and both components of light.[32–35] Furthermore, the development of a simultaneous control of amplitude and phase of light has been attempted in some studies, and plasmonic metasurfaces with V-shaped meta-atoms proposed; however, they have limited modulation ranges, sophisticated fabrication requirements, as well as low efficiency.[36] Metasurfaces with C-shaped meta-atoms have been demonstrated with terahertz waves,[37] but fabrication difficulty with their convoluted modulation schemes makes it hard to implement their scalable design for visible light. A reflective metasurface with single nanorods has been proposed to control both the amplitude and phase of near-infrared waves by changing the length and rotation of the nanrods.[38] However, the scheme of changing the length of the nanorod is solely based on the resonant property of the structures, which cannot be applied to broadband operations; moreover, this sort of modulation schemes based on the changes of the structure lengths require very precise control of the geometries at the nanoscale due to high susceptible resonances, which result in high inaccuracy and fabrication difficulties. Other types of metasurfaces have also been suggested, but within theoretical considerations with low practicality or restricted capabilities.[39,40] As a result, none of the metasurfaces have achieved the complete control of complex-amplitude in visible range with subwavelength resolution and broadband.

In this study, an advanced holographic metasurface has been proposed and experimentally demonstrated that enables full and broadband complex-amplitude modulation of visible light with subwavelength spatial resolution, which can achieve the most complete holograms reaching to ideal holography. As a building block, an X-shaped meta-atom is introduced based on the expanded concept of the Pancharatnam-Berry phase. The X-shaped meta-atom, which is made of polycrystalline silicon (Poly-Si), enables that full ranges of both amplitude and phase can be mapped and tailored by tuning the orientations of its two arms. Furthermore, the metasurface provides broadband and chiral operations due to the great feature of the Pancharatnam-Berry phase.[17,20,22,25,27,29,31,42–49] Due to simple and intuitive design strategy, the proposed metasurface is resistant to fabrication errors and shows high efficiency in the mid-visible region (40% at 532 nm). To the best of our knowledge, this is the first time that the completely complex-amplitude modulated holograms have been experimentally realized for visible light with subwavelength spatial resolutions, and this is expected to be a significant advancement in optical holographic technology and metamaterials.

Results and discussion

Theory of the metasurface with X-shaped meta-atoms

A schematic depicting the mechanism of the X-shaped meta-atoms is represented in Fig. 1a. At first, the key principle of the proposed meta-atom, the Pancharatnam-Berry phase, has been discussed. The Pancharatnam-Berry phase, or geometric phase, is one of the most useful phenomena to describe the phase profile of scattered light by spin-rotation coupling. The geometric-phase metasurfaces commonly consist of a unit-cell of a rectangular nanorod, which is composed of plasmonic or dielectric materials. As shown in the left side of Fig. 1a, electric dipole moments are induced parallel to the major axis of the nanorod when the circularly polarized light (σ) is normally incident to the nanorod. Herein, the parameter σ is selected as +1 or −1 for right or left circular polarization, respectively. The orientation angle (θ_1 with respect to x-axis) of the nanorod leads to time delay of the dipole excitation; this makes relative phase delay among the nanorods according to their own orientation angles. As a result, the scattered light with opposite

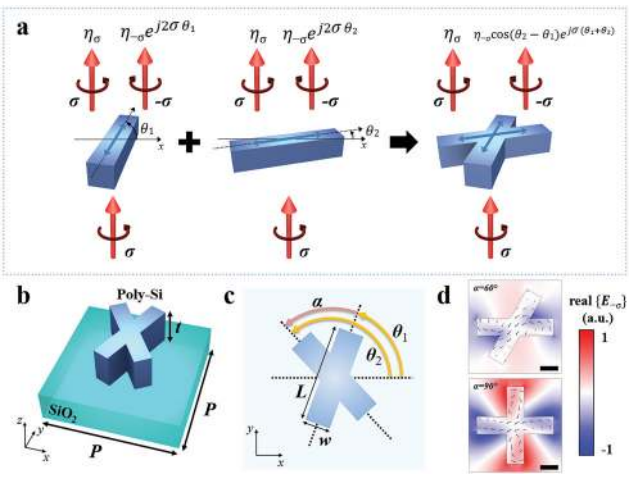

Fig. 1 Schematic of an X-shaped meta-atom (a) describing the operating mechanism of the structures. Rotation of the single nanorod with orientation angle θ_1 (or θ_2) leads to the phase variance $2\sigma\theta_1$ (or $2\sigma\theta_2$) in a cross-polarized component of transmitted light according to the Pancharatnam-Berry phase. The superposition of the two nanorods with different orientation angles θ_1 and θ_2 implements the X-shaped structure, which has the amplitude $2\cos(\theta_2 - \theta_1)$ and phase $\sigma(\theta_1 + \theta_1)$ in a cross-polarized component of transmitted light. η_σ and $\eta_{-\sigma}$ are the coupling coefficients of co- and cross-polarized light, respectively. (b) Schematic of a unit cell of the proposed metasurface. An X-shaped meta-atom consists of Poly-Si on a glass substrate with thickness t and the unit cell period P. (c) Top view of the unit cell showing longer length L, width w, orientation angles of its arms θ_1 and θ_2, and their disparity α. For the metasurfaces designed at the operating wavelength λ_d = 532 nm, X-shaped meta-atoms have L = 290 nm, w = 65 nm, t = 128 nm, and P = 350 nm. (d) Simulation results that show the distribution of electric fields and polarization vectors. Colours represent the real part of cross-polarized electric fields ($E_{-\sigma}$), and black arrows in the figures represent the magnitudes and directions of the polarization vectors at each position. The upper figure has the angular disparity α = 60°, whereas the lower figure has α = 90°. Other geometric parameters of both structures are identical. Scale bar, 50 nm.

handedness ($-\sigma$) experiences a relative phase shift ($2\sigma\theta_1$), which is only proportional to the orientation angle. The geometric phase is a purely geometrical effect, which can lead to broadband characteristics whose tendency of phase shift is independent of the wavelength of light.

In this regard, the concept of geometric phase can be expanded. If two nanorods with different orientation angles (θ_1 and θ_2) are overlapped, they will construct an X-shaped structure whose arms direct to the angles θ_1 and θ_2. Speculating that the X-shaped structure can be modelled by two independent electric dipoles, the behaviour of the X-shaped structure is allowed to be analysed by the superposition of the geometric phase. The phase components of cross-polarized waves scattered by these electric dipoles are just proportional to their orientation angles, but with the same amplitude components. Hence, the complex-amplitude of the cross-polarized wave (E_{cross}) radiated from the X-shaped structure can be simply expressed as follows:

$$E_{\text{cross}} \propto e^{j2\sigma\theta_2} + e^{j2\sigma\theta_1} = (e^{j\sigma(\theta_2-\theta_1)} + e^{-j\sigma(\theta_2-\theta_1)})e^{j\sigma(\theta_1+\theta_2)} = 2\cos(\theta_2-\theta_1)e^{j\sigma(\theta_1+\theta_2)} \quad (1)$$

According to eqn (1), the complex-amplitude E_{cross} can be separated into the amplitude and phase component. The amplitude A and phase ϕ of the total cross-polarized wave can be expressed as $2\cos(\theta_2 - \theta_1)$ and $\sigma(\theta_1 + \theta_2)$, respectively. That is, the amplitude of scattered light can be determined by the difference between two orientation angles, whereas the phase of scattered light can be determined by the summation of two orientation angles. Thus, we confirm that the complex-amplitude modulation can be realized from the double electric dipoles. However, in the case of an actual X-shaped structure, higher order modes, such as magnetic dipoles and electric quadrupoles, rather than the electric dipole modes can be excited when a circularly polarized light illuminates on the backside of the structure. However, we have found that these higher order modes can be suppressed, and only double electric dipoles are dominantly generated around the specific resonance. This resonance can occur with accurately designed geometric parameters such as thickness, length, and width of the X-shaped structure. Therefore, the proposed X-shaped structure can modulate the incoming light with the full coverage of complex-amplitude domain according to eqn (1).

Based on the theoretical analysis, the X-shaped meta-atoms were implemented using dielectric materials. A schematic of the proposed unit cell is shown in Fig. 1b. The meta-atom consists of poly-Si on a glass substrate with the thickness of t. The metasurface is then composed of periodically arranged square lattices of X-shaped meta-atoms with the period P for both x- and y-directions. The proposed structure is designed to operate in the visible light with the wavelength of 532 nm; thus, the period (P = 350 nm) is set to be shorter than the wavelength of light. Since the period is even shorter than the wavelength in the glass substrate with the refractive index of 1.45, there are no diffraction orders in both transmission and reflection. The thickness of poly-Si (t = 128 nm) is chosen to compose a Fabry–Perot resonator with a low quality-factor, which not only enhances the modulation efficiency but also allows broadband operations. Fig. 1c shows the top view of the unit cell. Each pixel has its own orientation angles (θ_1 and θ_2) about the x-axis. The angular disparity between the orientation angles is defined as α. Considering both the fabrication feasibility and modulation efficiency, other parameters, such as the length of the nanorod (L = 290 nm) and the width of the nanorod (w = 65 nm), were also carefully designed. Although only a transmission-type metasurface has been discussed herein, we have confirmed that a reflection-type metasurface can also be implemented in the same manner in the visible region (see the ESI Part 1†).

Verification with numerical simulations

The capability of the X-shaped meta-atom is verified by a commercial tool (COMSOL) based on the finite element method (FEM) (see the ESI Part 2† for details). Electric field maps of the X-shaped meta-atom with normal incidence of circular polarization were calculated first, as shown in Fig. 1d. Herein, two cases of X-shaped structures with α = 60° and 90° are considered as examples (for other cases, see Fig. S4 and S5†). In the figure, colours represent the real part of cross-polarized electric fields ($E_{-\sigma}$), whereas the black arrows represent the magnitude and directions of electric polarization vectors. It is noticeable that we have allowed the values of α to be in the range from 60° to 90° because a meta-atom having an α smaller than 60° is not appropriate to apply the superposition mechanism of the X-shaped structure due to severe overlap of two nanorods, which is not suitable for our theoretical approach. As shown in Fig. 1d, it can be confirmed that the electric dipoles are dominantly induced along the arms of the X-shaped meta-atom in the defined range; this means that the speculation of our theoretical approach is practically valid (see Fig. S4 and S5† for details).

Fig. 2 shows the cross-polarized transmission coefficient (t_{cross}) as a function of the orientation angle (θ_1) and the angular disparity (α) calculated from both theoretical calculations and FEM simulations. Herein, t_{cross} is defined as the ratio of complex-amplitude of the cross-polarized transmission (E_{cross}) to incident light (E_{in}), as depicted in Fig. 2a. Fig. 2b–d present the results of theoretical calculations based on eqn (1) that models the X-shaped meta-atom as double electric dipoles whose directions are parallel to the major axes of two arms. Corresponding FEM simulation results for the actual X-shaped meta-atom are presented in Fig. 2e–g. To compare the results in detail, they are represented separately in each component *i.e.* the amplitude (Fig. 2b and e) and phase (Fig. 2c and f). Fig. 2d and g describe all the t_{cross} in the complex domain whose x- and y-axes mean the real and imaginary part of the complex-amplitude, respectively. As expected, both results of modelling and simulations show a strong agreement. The angular disparity is related with the amplitude, whereas the orientation angle is related with the phase relying on the eqn (1). In addition, the simulation indicates that the maximum efficiency, which is defined as the efficiency for the maximized

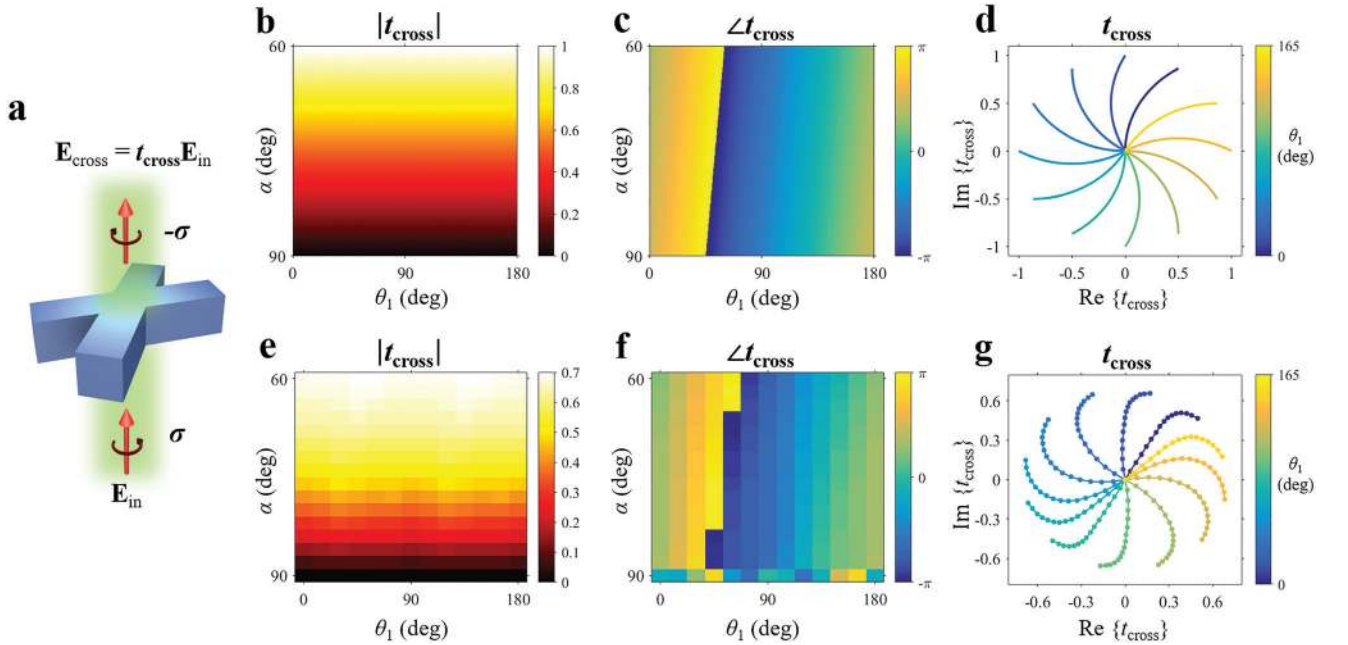

Fig. 2 Theoretical and numerical analyses of cross-polarized transmissions of an X-shaped meta-atom. (a) Schematic of a unit cell of an X-shaped meta-atom. Cross-polarized transmission coefficient t_{cross} is defined as the ratio between the complex amplitude of cross-polarized component of transmitted light and that of incident light. Results of (b–d) analytical calculations and (e–g) FEM simulations for t_{cross}. (b and e) Variation in the amplitude component of t_{cross} for different orientation angles θ_1 and disparities α. (c and f) Variation in the phase component of t_{cross} for different orientation angles θ_1 and disparities α. (d and g) Accessible range of t_{cross} plotted in the complex domain. The different colours of the lines represent the cases of different orientation angles, and the colour bar is represented on the right side of the graphs.

amplitude, reaches 49% at the wavelength of 532 nm. As a consequence, we can confirm that our theoretical approach is fairly accurate, and both amplitude and phase of transmitted and cross-polarized light can be fully described by the orientation angles of the two arms of the X-shaped meta-atom with high efficiency.

Experimental demonstrations of X-shaped metasurfaces

To experimentally demonstrate the extraordinary capability and versatility of the proposed metasurface, metasurfaces composed of X-shaped meta-atoms were fabricated according to the geometric parameters by standard electron beam lithography process (see the ESI Part 3† for details). In this section, we have characterized two different categories of the metasurfaces. The first category was a set of metasurfaces with a periodic array of identical X-shaped meta-atoms to measure transmission characteristics of the unit cell. The other category was used for validating the performance of full complex-amplitude holographic metasurfaces using X-shaped meta-atoms as compared to that of a phase-only holographic metasurface.

Herein, four devices belonging to the first category consist of identical X-shaped meta-atoms with four types of angular disparities: α = 60°, 70°, 80°, and 90°. Fig. 3a–d represent their field-enhanced scanning electron microscopy (FE-SEM) images. According to the images, it is possible to confirm the feasibility of the proposed structures at the nanoscale. The samples were then illuminated from the bottom by a laser with the free-space wavelength (λ_d) of 532 nm. On the transmitted side, a cross-polarized circular analyser comprising a quarter waveplate and a linear polarizer was used to filter and measure the cross-polarized component of transmitted light. Using the oppositely directional circular analyser comprising a quarter waveplate and a linear polarizer, the cross-polarized component of transmitted light can be measured. The results are shown in Fig. 3e with the simulation results. The intensity values in Fig. 3e are normalized by the case of α = 60°. According to the graph, both experiments and simulations indicate that the intensity of t_{cross} sinusoidally decreases when α increases from 60° to 90°, and finally, it reaches zero at α = 90°. For the maximum case of the experimental results, we measured a maximum efficiency of 40% in cross-polarized transmission. The measured efficiency is a bit smaller than its corresponding simulated values (49%) because of slight differences between the geometry of the designed and fabricated structures.

The second category of our metasurfaces was prepared for validating the functionalities of full complex-amplitude metasurface holograms. As abovementioned, extraordinary capability of X-shaped meta-atoms can satisfy the requirement of ideal complex-amplitude holograms. We designed the computer-generated holograms (CGHs) for right circularly polarized light with normal incidence. As shown in Fig. 4a, the CGHs were designed to generate the letters "SNU" in 3D space. The letters "S", "U", and "N" are displayed on different image planes in the Fresnel region, which are at z = 0 μm, 80 μm, and 150 μm, respectively. It is noticeable that one of the image

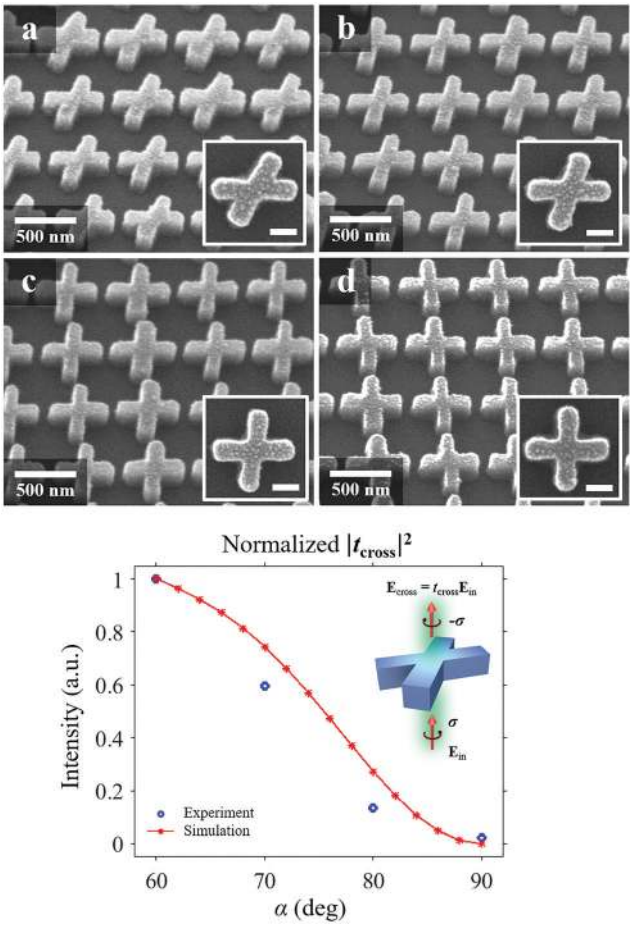

Fig. 3 Experimentally measured cross-polarized transmissions (t_{cross}) of the X-shaped meta-atoms in several angular disparities. (a–d) FE-SEM images of the metasurfaces composed of regularly patterned X-shaped unit-cells with the angular disparities α = 60°, 70°, 80°, and 90° for (a), (b), (c), and (d), respectively. Scale bar of inset, 50 nm. (e) Results of both simulations and experiments for the cross-polarized transmittance as a function of the angular disparity α. Blue circles indicate the experimental results, whereas the red-crossed points and curve are for the FEM simulation results. The results are normalized to the transmittance for the case of α = 60°, which is designed to have the maximum transmittance.

planes is located at z = 0 μm, which is directly on the metasurface plane, to show the unique performance of complex-amplitude holograms. For conventional phase-only holograms, only phase information of object images remains, whereas the amplitude information of them is set to be identical. Therefore, it is impossible to describe the images directly on the metasurface plane. On the other hand, complex-amplitude holograms have both amplitude and phase information, which is capable of describing the reconstructed images on arbitrary planes including the surface of metasurfaces. Therefore, the proposed example can definitely prove whether the given metasurfaces modulate the phase, amplitude, or both. Calculated CGHs with a sample size of 210 μm × 210 μm and a pixel size of 350 nm × 350 nm are shown in the upper side of Fig. 4d. Any approximations or algorithms, such as random phase injection, that should be used in conventional phase-only holograms are not employed to obtain the expected amplitude and phase profiles, and the back-propagation of the desired image profiles is taken into account according to the Fresnel diffraction theory. The optical microscopy image and FE-SEM images of the fabricated devices possessing the designed CGHs are shown in Fig. 4b and c, respectively. Fig. 4d shows the obtained holographic images at each z-plane in both simulations and experiments. Optical microscopy setup with the cross-polarized analyser was used to measure the holographic images (see the ESI Part 4† for details and Fig. S1† for the illustration of the setup). It is noteworthy that the holographic images of both simulations and experiments have almost identical profiles without any significant noises; this demonstrates the great capability of the metasurface for generating holographic images in 3D space. Moreover, the letter "S" reconstructed on the image plane very close to the metasurface is purely described; this indicates that the amplitude profiles as well as the phase profiles are correctly implemented. A signal-to-noise ratio (SNR), which is defined as the ratio of the maximum intensity in the holographic image to the standard deviation of the background noise,[36] has been used to evaluate the image quality. For the experimentally reconstructed image in Fig. 4d, the SNR is 211.3 where the background area is set to the size of 32 μm × 32 μm. This is a remarkable record since the SNRs reported in previous studies have only the values around 50 although approximation algorithms are used in them that improve the image quality, but sacrifice the original wavefronts.[36,44]

For comparison, the phase-only metasurface with uniform amplitude profiles was also designed, and the other conditions were the same as those of the sample shown in Fig. 4d. Due to the deficient expressiveness of phase-only holograms, multiplication of randomly valued phase profiles should be employed to improve the image quality of the phase-only holograms (see the ESI Part 5† for details). Calculated phase profile of the phase-only CGH is shown in the upper side of Fig. 4e. Both calculated and measured holographic images in Fig. 4e show that the letter "S" cannot be formed at the metasurface plane as properly as the other letters "N" and "U" are displayed due to severe noises around the images. Upon comparing the holographic images of Fig. 4d and e, we conclude that the complex-amplitude hologram can overcome the speckle noise problem of typical phase-only holograms, significantly expand the range of reconstructed image plane, and simplify the complicated calculation processes of the phase-only CGHs that often involve iterative algorithms.

Moreover, one of the attractive properties of the proposed metasurface is the broadband characteristic. As proved in the theoretical approach, the nature of the X-shaped meta-atoms originates from the geometric phase, which only depends on the orientation of the structure. In addition, the broadband characteristic of the proposed metasurface is more improved using all-dielectric materials, which have less sensitive resonance properties as compared to plasmonic materials with sharp plasmonic resonances.[41] Therefore, it is expected that

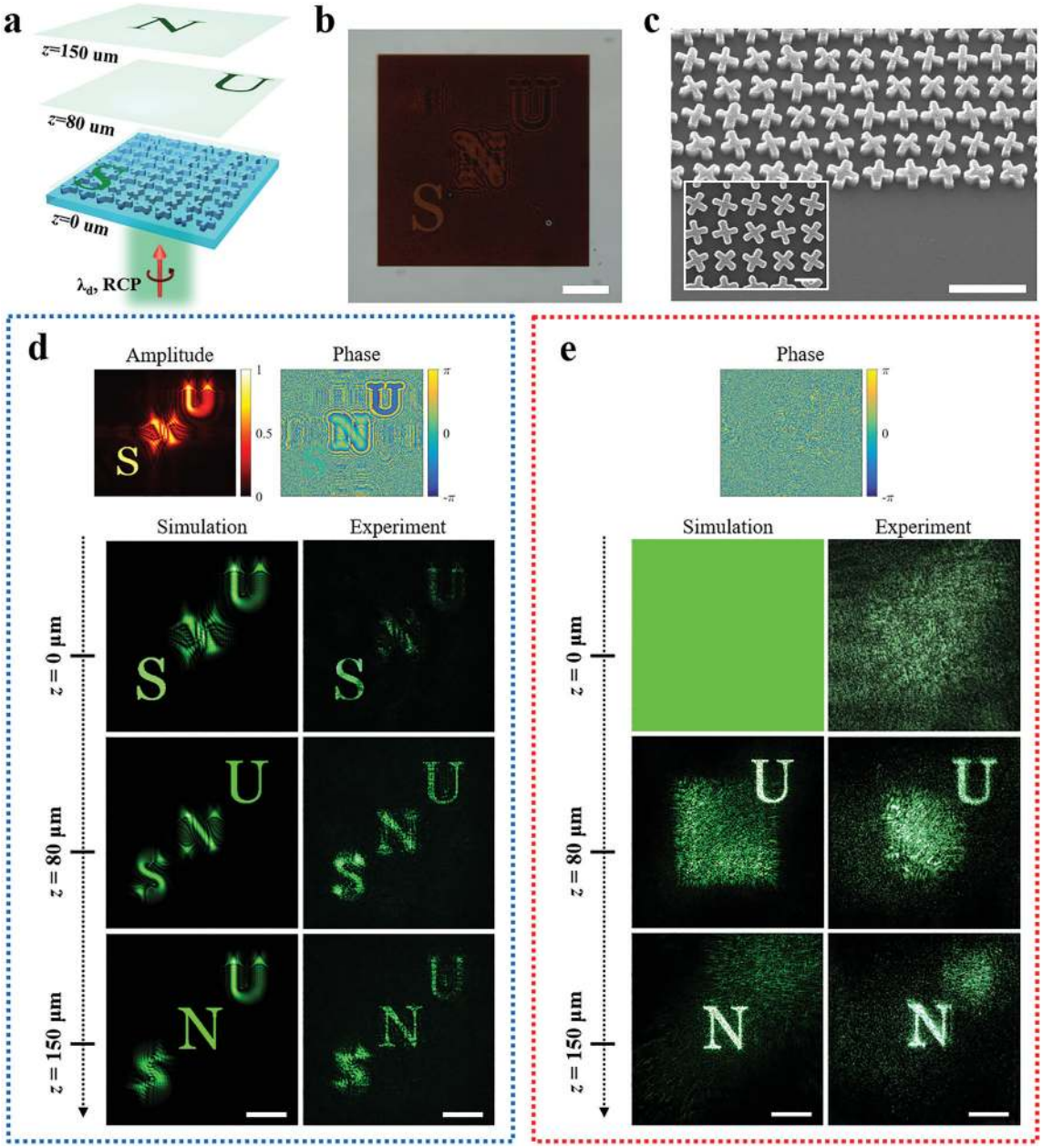

Fig. 4 Full complex-amplitude and phase-only holograms reconstructed by X-shaped metasurfaces. (a) Schematic for the designed hologram. The right circularly polarized light with the wavelength λ_d = 532 nm was used to reconstruct the hologram. The three letters "SNU" are reconstructed on the proper image planes that are on the metasurface plane for "S", *xy*-plane on the z = 80 μm for "U", and *xy*-plane on the z = 150 μm for "N". (b) Optical microscopy image of the fabricated device on the fused silica wafer. Scale bar, 50 μm. (c) FE-SEM images of the fabricated metasurfaces for the tilted view and top view (inset). Scale bars are 500 nm and 300 nm for the main and inset images, respectively. (d) Designed CGH and obtained holographic images of the complex-amplitude hologram. Amplitude and phase profiles of CGHs with 600 × 600 number of pixels are represented on the upper side. Calculated images and their corresponding measured intensity distributions at proper image planes are shown in the lower side. Continuous change of the holographic images with respect to z is shown in Movie S1† with explanation in Fig. S7.† Scale bar, 50 μm. (e) Designed phase-only CGH and obtained holographic images of the phase hologram. Calculated and measured intensity distributions are shown in the lower side, whereas the phase profile is shown in the upper side. Scale bar, 50 μm. Experimental images were obtained by a colour CCD camera.

phase and amplitude of cross-polarized transmission are relatively independent of the wavelength of the incident light. We performed the simulations to analyse the structures at different wavelengths (see Fig. S6†). Consequently, the phase is absolutely independent of the wavelength, and the amplitude also relies on the theory, but with a few fluctuations relying on the orientation of the structure for wavelengths longer than λ_d. These fluctuations are due to the interactions among adjacent unit cells where the interactions are hard to be ignored for different wavelengths, and they can be sufficiently corrected by

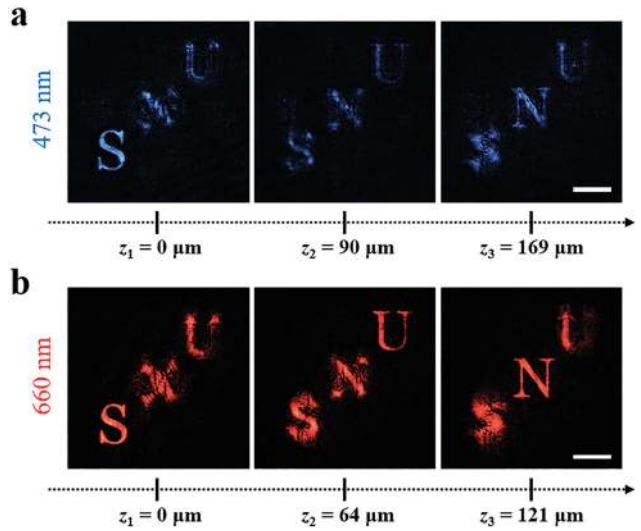

Fig. 5 Experimentally obtained holographic images for verifying the broadband characteristic of the X-shaped metasurface. Measured images at proper image planes for the wavelength of (a) 473 nm and (b) 660 nm. Positions of image planes are shown in the figures for each case. Their corresponding values of theoretical calculations at 473 nm are z_1 = 0 μm, z_2 = 90 μm, and z_3 = 169 μm, whereas the values at 660 nm are z_1 = 0 μm, z_2 = 64 μm, and z_3 = 121 μm. Continuous change of the holographic images with respect to z is shown in the Movie S2 and S3† with explanation in Fig. S7† for the wavelength of 473 nm and 660 nm, respectively. Scale bar, 50 μm.

scale optimizations of the geometry for desired wavelength regions. By the way, the main tendency of the complex-amplitude modulation is conserved for different wavelengths. The metasurface used for demonstrating a hologram shown in Fig. 4d was reused for experiments with different wavelengths of 660 nm and 473 nm, and the images at the preferred z-planes were obtained, as shown in Fig. 5. As expected, the holographic images were well reconstructed at each z-plane, whereas just z-positions of image planes were changed with respect to the operating wavelengths. The positions of the images can be theoretically calculated according to the principle of geometrical optics, and measured positions of image planes agree well with their corresponding calculations in all the wavelengths.

Conclusions

In summary, we have proposed a new type of metasurface composed of X-shaped meta-atoms to achieve full complex-amplitude modulation in the broadband visible wavelength region. Theoretically, the concept of geometric phase was expanded and applied to materialize an X-shaped meta-atom. Theoretical discussions and numerical simulations of the X-shaped meta-atom have verified that both phase and amplitude of light can be spatially controlled in the range of 0–1 for amplitude and 0–2π for phase within a subwavelength resolution (350 nm × 350 nm). Experiments with regularly patterned metasurfaces showed a feasibility and a precise modulation capability of the X-shaped meta-atom. The maximum efficiency of 49% in simulation and 40% in experiment for cross-polarized transmission were achieved at the wavelength of 532 nm. Our selected material, poly-Si, has the benefits of high efficiency as well as standard fabrication processes with low cost. By applying the metasurface to transmission-type and on-axis holograms, a complete hologram was achieved experimentally with arbitrary complex-amplitude profiles in the broadband visible wavelengths. The extraordinary capability of the complex-amplitude hologram has also been discussed as compared to that of the phase-only hologram. According to the results, it was confirmed that the complex-amplitude hologram could provide excellent 3D images and absolutely eliminate the speckle noise problems of classical hologram where the experimental SNR was valued at 211.3.

A great advantage of the X-shaped meta-atom is its applicability for extensive fields of metasurface platforms based on the geometric phase. Broadband and chirality of the geometric phase have been applied to numerous functional metasurfaces. Polarization-multiplexed holographic imaging,[42–44] chiral and multispectral imaging,[45] and multi-functional flat optic devices[31,46–49] are achieved using the nature of the geometric phase. Because the X-shaped meta-atom originates from the geometric phase, it is worth mentioning that the proposed X-shaped meta-atom can also be applied to all the previous approaches using the nature of the geometric phase. In addition, it can improve their performances and has a potential to add a novel degree of freedom to these applications. Although visible light has been mainly discussed in this study due to its significance in holographic imaging, the operation range of the metasurface is also scalable to other wavelengths such as near-, mid-infrared, and terahertz regions.

We conclude that the modulation capability of the proposed metasurface as well as its aforementioned advantages almost reached those of the ideal 3D holograms. Moreover, our metasurface platform can be applied to not only holographic imaging but also to a wide spread of optical applications. The extraordinary degree of freedom achieved herein for controlling the electromagnetic waves can expand the superior limits of various optical applications including arbitrary beam shaping, 3D biological imaging, optical computing, integrated fibre-optics, and nanolasers. Ultimately, a perfect control of light, which means full and simultaneous control of amplitude, phase and polarization of light with subwavelength resolution, is expected to be achieved by applying this study.

Conflicts of interest

There are no conflicts of interest to declare.

Acknowledgements

This work was supported by the Center for Advanced Meta-Materials (CAMM) funded by the Ministry of Science, ICT and Future Planning as Global Frontier Research Project

(CAMM-2014 M3A6B3063710, CAMM-2014 M3A6B3063708). The authors acknowledge the support received from the Brain Korea 21 (BK21) project. J. R. acknowledges the financial supports received from the LGD-SNU Incubation program funded by LG Display, and Green Science program funded by POSCO, NRF Young Investigator program (NRF-2015R1C1A1A02036464) funded by the Ministry of Science, ICT and Future Planning (MSIP) of Korean government.

References

1 J. W. Goodman, *Introduction to Fourier Optics*, Robert & Company Publisher, Englewood, 2005.
2 P.-A. Blanche, A. Bablumian, R. Voorakaranam, C. Christenson, W. Lin, D. Gu, D. Flores, P. Wang, W.-Y. Hsieh, M. Kathaperumal, B. Rachwal, O. Siddiqui, J. Thomas, R. A. Norwood, M. Yamamoto and N. Peyghambarian, *Nature*, 2010, **468**, 80–83.
3 J. Geng, *Adv. Opt. Photonics*, 2013, **5**, 456–535.
4 B. Lee, *Phys. Today*, 2013, **66**, 36.
5 E. Noponen and J. Turunen, *J. Opt. Soc. Am. A*, 1996, **7**, 1422–1428.
6 L. G. Neto, D. Roberge and Y. Sheng, *Appl. Opt.*, 1996, **35**, 4567–4576.
7 J. L. de Bougrenet de la Tocnaye and L. Dupont, *Appl. Opt.*, 1997, **8**, 1730–1741.
8 E. Ulusoy, L. Onural and H. M. Ozaktas, *J. Opt. Soc. Am. A*, 2011, **28**, 2310–2321.
9 X. Li, J. Liu, J. Jia, Y. Pan and Y. Wang, *Opt. Express*, 2013, **21**, 20577–20587.
10 J. B. Pendry, D. Schurig and D. R. Smith, *Science*, 2006, **312**, 1780–1782.
11 N. Yu and F. Capasso, *Nat. Mater.*, 2014, **13**, 139–150.
12 N. Meinzer, W. L. Barnes and I. R. Hooper, *Nat. Photonics*, 2014, **8**, 889–898.
13 A. I. Kuznetsov, A. E. Miroshnichenko, M. L. Brongersma, Y. S. Kivshar and B. Luk'yanchuk, *Science*, 2016, **354**, aag2472.
14 S. Jahani and Z. Jacob, *Nat. Nanotechnol.*, 2016, **11**, 23–36.
15 D. R. Smith, J. B. Pendry and M. C. K. Wiltshire, *Science*, 2004, **305**, 788–792.
16 V. M. Shalaev, *Nat. Photonics*, 2007, **1**, 41–48.
17 G. Li, S. Chen, N. Pholchai, B. Reineke, P. W. H. Wong, E. Y. B. Pun, K. W. Cheah, T. Zentgraf and S. Zhang, *Nat. Mater.*, 2015, **14**, 607–612.
18 M. R. Shcherbakov, D. N. Neshev, B. Hopkins, A. S. Shorokhov, I. Staude, E. V. Melik-Gaykazyan, M. Decker, A. A. Ezhov, A. E. Miroshnichenko, I. Brener, A. A. Fedyanin and Y. S. Kivshar, *Nano Lett.*, 2014, **14**, 6488–6492.
19 K. O'Brien, H. Suchowski, J. Rho, A. Salandrino, B. Kante, X. Yin and X. Zhang, *Nat. Mater.*, 2015, **14**, 379–383.
20 D. Lin, P. Fan, E. Hasman and M. L. Brongersma, *Science*, 2014, **345**, 298–302.
21 P. Genevet and F. Capasso, *Rep. Prog. Phys.*, 2015, **78**, 024401.
22 G. Zheng, H. Muhlenbernd, M. Kenney, G. Li, T. Zentgraf and S. Zhang, *Nat. Nanotechnol.*, 2015, **10**, 308–312.
23 M. I. Shalaev, J. Sun, A. Tsukernik, A. Pandey, K. Nikolskiy and N. M. Litchinitser, *Nano Lett.*, 2015, **15**, 6261–6266.
24 J. Jin, P. Genevet, M. A. Kats, N. Antonious and F. Capaaso, *Nano Lett.*, 2013, **13**, 4269–4274.
25 L. Huang, X. Chen, H. Muhlenbernd, G. Li, B. Bai, Q. Tan, G. Jun, T. Zentgraf and S. Zhang, *Nano Lett.*, 2012, **12**, 5750–5755.
26 Y. F. Yu, A. Y. Zhu, R. Paniagua-Dominguez, Y. H. Fu, B. Luk'yanchuk and A. I. Kuzneetsov, *Laser Photonics Rev.*, 2015, **9**, 412–418.
27 K. Huang, Z. Dong, S. Mei, L. Zhang, Y. Liu, H. Liu, H. Zhu, J. Teng, B. Luk'yanchuk, J. K. W. Yang and C.-W. Qiu, *Laser Photonics Rev.*, 2016, **10**, 500–509.
28 X. Ni, S. Ishii, A. V. Kildishev and V. M. Shalaev, *Light: Sci. Appl.*, 2013, **2**, e72.
29 L. Huang, X. Chen, H. Muhlenbernd, H. Zhang, S. Chen, B. Bai, Q. Tan, G. Jun, K.-W. Cheah, C.-W. Qiu, J. Li, T. Zentgraf and S. Zhang, *Nat. Commun.*, 2013, **4**, 2808.
30 A. Arbabi, Y. Horie, A. J. Ball, M. Bagheri and A. Faraon, *Nat. Commun.*, 2015, **6**, 7069.
31 P. C. Wu, W.-Y. Tsai, W. T. Chen, Y.-W. Huang, T.-Y. Chen, J.-W. Chen, C. Y. Liao, C. H. Chu, G. Sun and D. P. Tsai, *Nano Lett.*, 2017, **17**, 445–452.
32 A. Arbabi, Y. Hoie, M. Bagheri and A. Faraon, *Nat. Nanotechnol.*, 2015, **10**, 937–943.
33 J. Li, S. Chen, H. Yang, J. Li, P. Yu, H. Cheng, C. Gu, H.-Y. Chen and J. Tian, *Adv. Funct. Mater.*, 2015, **25**, 704–710.
34 J. Park, J. H. Kang, S. J. Kim, X. Liu and M. L. Brongersma, *Nano Lett.*, 2017, **17**, 407–413.
35 J. P. B. Mueller, N. A. Rubin, R. C. Devlin, B. Groever and F. Capasso, *Phys. Rev. Lett.*, 2017, **118**, 113901.
36 X. Ni, A. V. Kildishev and V. M. Shalaev, *Nat. Commun.*, 2015, **4**, 2807.
37 L. Liu, X. Zhang, M. Kenney, X. Su, N. Xu, C. Ouyang, Y. Shi, J. Han, W. Zhang and S. Zhang, *Adv. Mater.*, 2014, **26**, 5031–5036.
38 M. Kim, A. M. H. Wong and G. V. Eleftheriades, *Phys. Rev. X*, 2014, **4**, 041042.
39 E.-Y. Song, G.-Y. Lee, H. Park, K. Lee, J. Kim, J. Hong, H. Kim and B. Lee, *Adv. Opt. Mater.*, 2017, **5**, 1601028.
40 F. Monticone, N. M. Estakhri and A. Alù, *Phys. Rev. Lett.*, 2013, **110**, 203903.
41 S. A. Maier, *Plasmonics: Fundamentals and Applications*, Springer, New York, 2007.
42 D. Wen, S. Chen, F. Yue, K. Chan, M. Chen, M. Ardron, K. F. Li, P. W. H. Wong, K. W. Cheah, E. Y. B. Pun, G. Li, S. Zhang and X. Chen, *Adv. Opt. Mater.*, 2016, **4**, 321–327.
43 L. Huang, H. Muhlenbernd, X. Li, Xu. Song, B. Bai, Y. Wang and T. Zentgraf, *Adv. Mater.*, 2015, **27**, 6444–6449.
44 D. Wen, F. Yue, G. Li, G. Zheng, K. Chan, S. Chen, M. Chen, K. F. Li, P. W. H. Wong, K. W. Cheah, E. Y. B. Pun, S. Zhang and X. Chen, *Nat. Commun.*, 2015, **6**, 8241.

45 M. Khorasaninejad, W. T. Chen, A. Y. Zhu, J. Oh, R. C. Devlin, D. Rousso and F. Capasso, *Nano Lett.*, 2016, **16**, 4595–4600.
46 X. Chen, L. Huang, H. Muhlenbernd, G. Li, B. Bai, Q. Tan, G. Jin, C.-W. Qiu, S. Zhang and T. Zentgraf, *Nat. Commun.*, 2012, **3**, 1198.
47 L. Huang, X. Song, B. Reineke, T. Li, X. Li, J. Liu, S. Zhang, Y. Wang and T. Zentgraf, *ACS Photonics*, 2017, **4**, 338–346.
48 M. Khorasaninejad, W. T. Chen, R. C. Devlin, J. Oh, A. Y. Zhu and F. Capasso, *Science*, 2016, **352**, 1190.
49 M. Khorasaninejad, W. T. Chen, J. Oh and F. Capasso, *Nano Lett.*, 2016, **16**, 3732–3737.